J. Fluid Mech. (2005), *vol.* 536, *pp.* 209–218. © 2005 Cambridge University Press
doi:10.1017/S0022112005005112 Printed in the United Kingdom

On two-dimensional temporal modes in spatially evolving open flows: the flat-plate boundary layer

By UWE EHRENSTEIN AND FRANÇOIS GALLAIRE

Laboratoire J. A. Dieudonné, Université de Nice-Sophia Antipolis,
Parc Valrose, F-06108 Nice Cedex 02, France
uwe.ehrenstein@unice.fr

(Received 28 January 2005 and in revised form 28 April 2005)

Temporal linear stability modes depending on two space directions are computed for a two-dimensional boundary-layer flow along a flat plate. The spatial structure of each individual temporally stable mode is shown to be reminiscent of the spatial exponential growth of perturbations along the flat plate, as predicted by local analyses. It is shown using an optimal temporal growth analysis, that an appropriate superposition of a moderate number of temporal modes gives rise to a spatially localized wave packet, starting at inflow and exhibiting transient temporal growth when evolving downstream along the plate. This wave packet is in qualitative agreement with the convectively unstable disturbance observed when solving the Navier–Stokes equations for an equivalent initial condition.

1. Introduction

The classical approach when considering hydrodynamic linear stability of weakly non-parallel open flows is to use the locally parallel flow assumption in the downstream direction and stability modes depend only on one space variable, the wall-normal direction. An exhaustive review of the dynamics that may be extracted from local analyses can be found in Huerre & Monkewitz (1990). Weakly non-parallel analyses may however fail when flow disturbances have length scale comparable with that of the basic flow. A separation of variables in the linear stability equations is then questionable and modes have to be considered which depend on both the wall-normal and streamwise direction. The resulting large numerical matrix eigenvalue problem becomes much less tractable. A way to overcome this difficulty is to use the time-marching algorithm for solving the Navier–Stokes system to compute the linear evolution of the disturbance about the basic flow, together with a Krylov subspace method (Edwards *et al.* 1994), which allows computation of a significant part of the spectrum. This approach has for instance been applied by Barkley, Gomes & Henderson (2002) to compute global critical eigenmodes localized in the separation bubble for highly non-parallel backward-facing step flow at moderate Reynolds numbers. With increasing computer capacities, the more direct approach of computing two-dimensional disturbance modes as matrix-eigenmodes of the discretized linearized Navier–Stokes equations is now feasible and has been applied with success for instance to wall-bounded flows by Lin & Malik (1997) who considered a non-parallel attachment-line boundary layer, or to separated recirculation bubbles in the work of Theofilis, Hein & Dallmann (2000). A recent review, with numerous references therein, of the state of the art concerning global linear instability analyses and the

different ways to numerically determine temporal modes depending on more than one space variable has been given by Theofilis (2003).

Two-dimensional temporal modes are expected to remain relevant even when the flow is only mildly non-parallel, as a consequence of the peculiar non-normality associated with their advection (see Chomaz 2005 for a review). Considering the model problem of the Ginzburg–Landau operator with spatially varying coefficients, Cossu & Chomaz (1997) have demonstrated that the non-normality of the streamwise global eigenmodes may lead to transient growth, which can be interpreted in terms of local convective instability. In this context, the one-dimensional global modes in the streamwise inhomogeneous direction can be viewed as models of the two-dimensional temporal global modes considered in the present paper. More recently, this idea has been applied to the stability of a falling liquid curtain modelled as a partial differential system with one inhomogeneous space variable by Schmid & Henningson (2002). An optimal superposition of temporal global modes reproduces the unstable wave packet evolving through the curtain, close to experimental observations. In the present investigation, we readdress the possibility of triggering convectively unstable wave packets using temporal two-dimensional modes. The flat-plate boundary layer is considered, as the archetype of a non-parallel wall-bounded shear flow.

2. Mathematical formulation and solution procedure

The basic flow state along a flat plate has been computed using the two-dimensional Navier–Stokes system, using a fourth-order finite-difference discretization in the streamwise x-direction and Chebyshev-collocation in the wall-normal y-direction. The underlying algorithm has been described in Marquillie & Ehrenstein (2003). The reference length is the displacement thickness δ_i^* at inflow x_i^*, the Blasius profile providing the inflow condition for the Navier–Stokes integration, and the uniform velocity U_∞^* at $y \to \infty$ is the reference velocity. The Reynolds number hence is written

$$Re = \frac{U_\infty^* \delta_i^*}{\nu^*} = \gamma \sqrt{\frac{U_\infty^* x_i^*}{\nu^*}}, \quad \gamma = 1.7208, \tag{2.1}$$

the viscosity being ν^*. Basic states $(U(x, y), V(x, y))$ have been computed for inflow Reynolds numbers of $Re = 610$ and $Re = 780$ above the critical Reynolds number $Re_c \approx 520$ for the Blasius profile, in the domain $x_i \leqslant x \leqslant x_o$ and $0 \leqslant y \leqslant y_{max}$ with $y_{max} \to \infty$. The length of the domain in the streamwise direction in the simulation was $x_o - x_i = 600$ with a finite-difference discretization of $N_x = 3000$ points. In the wall-normal direction an algebraic transformation has been used with $y_{max} = 80$ and $N_y = 100$ Chebyshev-collocation points for discretization.

Once a steady state $\boldsymbol{U}(x, y) = (U(x, y), V(x, y))$ is obtained, the Navier–Stokes system is linearized, considering a disturbance in the flow field and pressure

$$\boldsymbol{u}(x, y, t) = \hat{\boldsymbol{u}}(x, y)\, \mathrm{e}^{-\mathrm{i}\omega t}, \quad p(x, y, t) = \hat{p}(x, y)\, \mathrm{e}^{-\mathrm{i}\omega t}, \tag{2.2}$$

where $\hat{\boldsymbol{u}}(x, y) = (\hat{u}(x, y), \hat{v}(x, y))$, a solution of the partial differential system

$$-(\boldsymbol{U} \cdot \nabla)\hat{u} - (\hat{\boldsymbol{u}} \cdot \nabla)U - \frac{\partial \hat{p}}{\partial x} + \frac{1}{Re}\nabla^2 \hat{u} = -\mathrm{i}\omega \hat{u}, \tag{2.3}$$

$$-(\boldsymbol{U} \cdot \nabla)\hat{v} - (\hat{\boldsymbol{u}} \cdot \nabla)V - \frac{\partial \hat{p}}{\partial y} + \frac{1}{Re}\nabla^2 \hat{v} = -\mathrm{i}\omega \hat{v}, \tag{2.4}$$

$$\nabla \cdot \hat{\boldsymbol{u}} = 0. \tag{2.5}$$

The type of discretization used to recover the basic state when solving the Navier–Stokes equations is of course not suitable for solving the stability system (2.3)–(2.5): the resulting matrix-eigenvalue problem would be enormous. Since the use of Chebyshev polynomials provides the most efficient expansion of regular functions in terms of polynomials (Peyret 2002), we have considered an interpolation of the basic flow state and its derivatives on a Chebyshev-collocation grid in both space variables, in order to solve the stability problem in the domain $0 \leqslant x \leqslant L$, $0 \leqslant y \leqslant H$, where we place the inflow at $x = 0$ for convenience. The collocation points are defined in $[-1, 1] \times [-1, 1]$ and a simple linear stretching of the variables has been considered to map the physical domain into the computational one.

2.1. *Boundary conditions*

The upper limit H in the wall-normal variable has been chosen to be $H = 15$, that is 15 times the displacement thickness at inflow. One may hence be confident that the disturbance flow velocity field vanishes at this height $y = H$ and at the wall $y = 0$ the no-slip condition applies.

Physical meaningful in- and outflow conditions however are not straightforward. Dirichlet-type or Neumann-type boundary conditions apply when global modes are spatially localized. Here, the basic flow field is locally unstable over the whole domain and the disturbance mode structure will extend from inflow to outflow boundaries. Conditions which match approximations of the local dispersion relation at inflow and outflow appear to be more appropriate for the present case. The local profile at inflow is the Blasius profile and the local dispersion relation $\alpha(\omega)$, under the locally parallel flow assumption, can easily be determined by solving the Orr–Sommerfeld-type one-dimensional stability equation: the mode then is written $\boldsymbol{u}(x, y, t) = \hat{\boldsymbol{u}}(y)\, \mathrm{e}^{\mathrm{i}(\alpha x - \omega t)}$. At inflow the Reynolds number Re of the global stability analysis is to be considered whereas at outflow $x = L$ the local stability analysis, using the Blasius profile, has to be performed at

$$Re_L = Re\sqrt{1 + \frac{\gamma^2 L}{Re}} \tag{2.6}$$

by (2.1), when considering the boundary-layer similarity solution for the local analysis. The streamwise derivative of the global mode is matched with the local analysis at inflow and ouflow through the Robin boundary condition

$$\frac{\partial \boldsymbol{u}}{\partial x} = \mathrm{i}\alpha \boldsymbol{u}. \tag{2.7}$$

The local dispersion relation $D(\alpha, \omega) = 0$ provides a nonlinear relationship between the complex wavenumber and frequency. First, a real frequency ω_0 is chosen within the unstable frequency range at inflow as well as outflow and the local spatial stability analysis is performed. A linear approximation is then given by a Gaster-type transformation (Gaster 1962)†

$$\alpha \approx \alpha_{0,r} + \frac{\partial \alpha_r}{\partial \omega_r}(\omega_0)\,(\omega - \omega_0) \cdots \tag{2.8}$$

which is justified as long as the imaginary parts of α and ω are small. Indeed, the results below (cf. figure 1) justify this hypothesis *a posteriori*. It appears that the

† Note that the reference time being δ_i^*/U_∞^*, the local frequency $\omega_L = (Re_L/Re)\omega$ is to be considered at outflow.

results are essentially independent of the precise value ω_0. This finally leads to

$$-c_0\frac{\partial \boldsymbol{u}}{\partial x} - \mathrm{i}(\omega_0 - c_0\,\alpha_{0,r})\boldsymbol{u} = -\mathrm{i}\omega\boldsymbol{u} \quad \text{with} \quad c_0 = \frac{1}{(\partial\alpha_r/\partial\omega_r)(\omega_0)} \tag{2.9}$$

at inflow $x = 0$ and outflow $x = L$.

Concerning the pressure, its value on the boundary is given implicitly through the incompressibility condition (2.5) which is imposed in the interior of the domain as well as on the boundary. Spurious pressure modes, making the left-hand side of (2.3)–(2.5) singular, are inherent when a Chebyshev–Chebyshev discretization is used in a rectangular box (Peyret 2002). Once the four corner points are eliminated, there remain four spurious pressure modes, which are dealt with by prescribing explicit boundary conditions for the pressure on four points on the upper and lower boundary immediately adjacent to the corners. Since the pressure is defined up to a constant, one of these points is used to fix this constant. Homogeneous Neumann boundary conditions are imposed at the three remaining points. Indeed, at $y = H$ and $y = 0$, this condition provides a meaningful approximation of (2.3), (2.4) since the advective terms vanish and the diffusive terms are effectively small at the Reynolds numbers considered.

2.2. *Eigenvalue solver*

Despite the interpolation procedure, the generalized matrix eigenvalue problem obtained after interpolation consists of up to 25 000 complex equations which is still too large to be solved by standard QZ algorithms. The eigenvalue problem obtained after discretization may be written formally as

$$\boldsymbol{A}z = -\mathrm{i}\omega\boldsymbol{B}z, \tag{2.10}$$

the vector z containing the disturbance flow velocity and pressure. Krylov subspace projections provide the possibility of recovering most of the spectrum using the 'shift and invert' strategy. Details of the method are given for instance in Nayar & Ortega (1993) and the usefulness of this approach for global hydrodynamic stability analyses is discussed in Theofilis (2003). The complexity reduces to the computation of the Krylov subspace together with the Arnoldi algorithm applied to the eigenvalue problem

$$(\boldsymbol{A} - \lambda\boldsymbol{B})^{-1}\,\boldsymbol{B}z = \mu z, \quad \text{with} \quad \mu = \frac{1}{-\mathrm{i}\omega - \lambda}\,. \tag{2.11}$$

However, this does not necessitate the inversion of a matrix operator. Indeed, the Krylov subspace may be computed by a successive resolution of linear systems with matrix $(\boldsymbol{A} - \lambda\boldsymbol{B})$, using an LU decomposition, which is achievable even for a very large matrix. The algorithm leads to an $m \times m$ matrix whose eigenvalues approximate those of (2.11). A large part of the spectrum can be recovered with great accuracy when considering a large Krylov subspace. Here, we considered reduced systems, the eigenvalues being determined using a QZ-algorithm, with up to $m = 800$ equations. The operator is shifted in order to provide the spectrum in a quite large neighbourhood of the shift parameter λ. In most of the computations we set $\lambda = 0$. Given the large Krylov subspace we considered, the part of the spectrum relevant for our analysis could be recovered in one computation which took about 2 hours CPU on the NEC/SX5 (the code running at 3.3 Gflops).

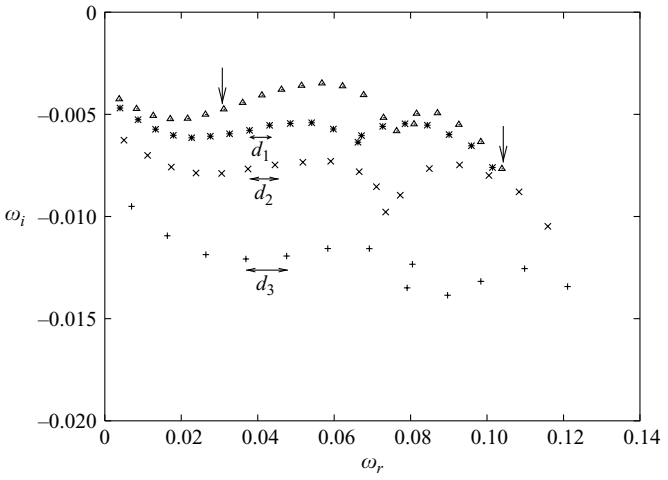

FIGURE 1. Eigenvalue spectrum in the (ω_r, ω_i)-plane for different Reynolds numbers and plate lengths. +, $Re = 610$ and $L = 230$; ×, $Re = 610$ and $L = 345$; ∗, $Re = 610$ and $L = 460$; △, $Re = 780$ and $L = 460$. The eigenmodes associated with the eigenvalues indicated by vertical arrows are depicted in figure 2.

3. Two-dimensional temporal modes and their superposition

For the two Reynolds numbers $Re = 610$ and 780 considered in the present analysis it has been checked that a Chebyshev-collocation discretization with $n_x = 180$ points in x and $n_y = 45$ points in y gives reasonably converged results when performing the global stability analysis for a domain length L up to $L = 460$. For the boundary conditions (2.9) at inflow and outflow, the expansion has been performed at $\omega_0 = 0.08$. The results proved to be quite insensitive to this parameter.

3.1. *Spectrum*

Several families of eigenvalue spectra are depicted in figure 1. From the spectrum obtained from the algorithm, the eigenvalues with highest imaginary parts, that is the least stable ones, are selected and a check of the two-dimensional mode structure allows elimination of spurious modes. It is seen that the individual global modes are stable with negative imaginary parts of ω as expected, the flat-plate boundary layer being convectively unstable. For the spectrum at $Re = 780$ and with $L = 460$, the eigenmode structures for the modes with $\omega_r \approx 0.03$ and $\omega_r \approx 0.1$ (marked with arrows in figure 1) are shown in figure 2. To better reveal the structure the aspect ratio between the x- and y-coordinates has been modified and the domain limited to $160 \leqslant x \leqslant 460$ and $0 \leqslant y \leqslant 12$. Isolines of the real part of the streamwise component $\hat{u}(x, y)$ are depicted and the perturbation is seen to evolve in the vicinity of the wall, with increasing amplitudes when progressing downstream. The typical length scale of the cellular mode structure decreases with increasing frequency, which introduces a cut-off in frequency for the spectrum.

The spectra shown in figure 1 are discrete, the separation between two successive frequencies being quite regular within each family of modes. To quantify this discretization of modes, for $Re = 610$ three different domain lengths have been considered with $L_1 = 460$, $L_2 = 345$ and $L_3 = 230$. Measuring the gap between two successive frequencies in the vicinity of $\omega_r = 0.04$ (cf. figure 1), one finds respectively for decreasing L, $d_1 = 0.0052$, $d_2 = 0.0071$ and $d_3 = 0.011$ and hence $d_2/d_1 \approx 1.36 \approx L_1/L_2$,

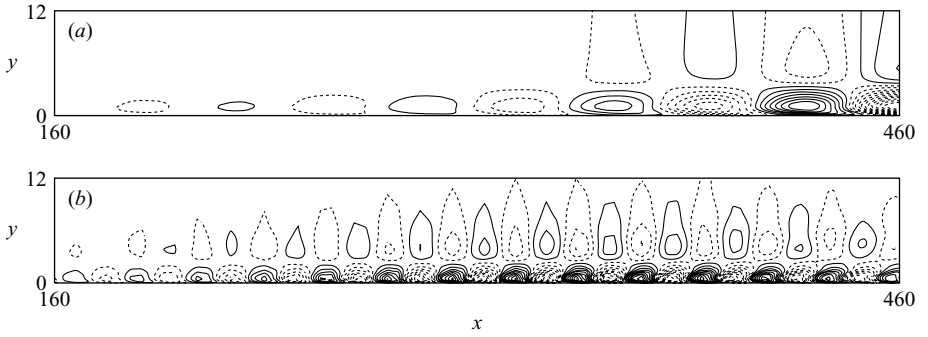

FIGURE 2. Isolines of the real part of $\hat{u}(x, y)$ of the two eigenmodes associated with the eigenvalues marked with arrows in figure 1 with (*a*) $\omega_r \approx 0.03$; (*b*) $\omega_r \approx 0.1$.

as well as $d_3/d_1 \approx 2.1 \approx L_1/L_3$. This kind of mode separation is believed to be due to the pressure. Indeed, taking into account the incompressibility condition, one may form a Poisson equation for the pressure by applying the gradient to equations (2.3), (2.4), the boundary condition of which being implicitly related to the incompressibility condition on the boundary. The resulting compatibility condition between inflow and outflow through the pressure discretizes the frequencies proportionally to $1/L$, the proportionality factor varying due to non-parallel effects.

The spatial structure of the two-dimensional temporal modes exhibits a growth in amplitude when progressing downstream, which may be quantified by computing

$$A(x) = \sqrt{\int_0^H (\hat{u}^*(x, y)\hat{u}(x, y) + \hat{v}^*(x, y)\hat{v}(x, y))\, \mathrm{d}y}, \tag{3.1}$$

where * denotes the complex conjugate. This spatial growth may be compared to the amplitude growth due to convective instability, as predicted by the locally parallel flow assumption. The complex wavenumber α_x is computed as function of the complex frequency at successive streamwise locations x. The Blasius profile is used for the one-dimensional stability problem, with the local Reynolds numbers Re_x as given by (2.6) with x instead of L and the local dimensionless frequency is $\omega_x = \omega Re_x/Re$. Neglecting the distortion of the wall-normal mode structure along x according to the so-called e^N method, integration of this factor provides the amplitude growth

$$\frac{A(x)}{A(0)} = \exp\left(\int_0^x -\alpha_{i,x}\, \mathrm{d}x\right). \tag{3.2}$$

The comparison between the streamwise global mode growth and the locally parallel flow prediction has been performed at two frequencies $\omega = 0.031 - \mathrm{i}\ 0.0048$ and $\omega = 0.104 - \mathrm{i}\ 0.0077$ marked with arrows in figure 1. The corresponding $A(x)/A(0)$ are compared in figure 3. The trends are the same for both the global-mode structure and the locally parallel approximation, which means that the two-dimensional mode structure is reminiscent of the spatial convective instability as given by local spatial instability theory.

3.2. *Mode superposition and wave packet*

The individual two-dimensional modes are stable but an appropriate superposition may exhibit a transient growth, the modes being non-normal. This type of behaviour was observed by Cossu & Chomaz (1997) when considering one-dimensional

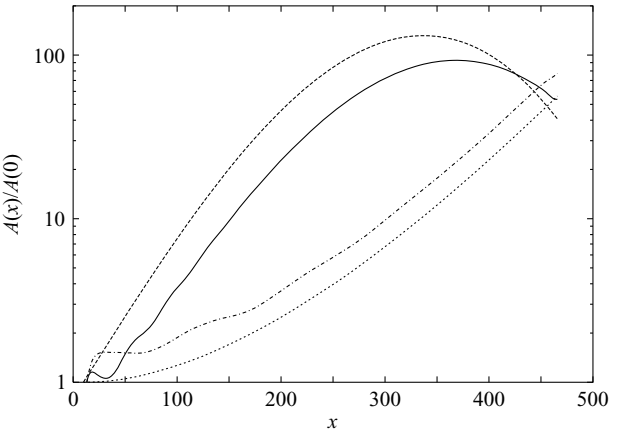

FIGURE 3. Normalized amplitude $A(x)/A(0)$ as function of the streamwise distance x of the two eigenmodes depicted in figure 2. Dotted-dashed line: mode in figure 2(a); continuous line: mode in figure 2(b). Comparison with the weakly non-parallel estimation (3.2) (dotted and dashed lines respectively).

streamwise modes associated with a model Ginzburg–Landau equation as a typical amplitude equation. Here, in the two-dimensional temporal setting, the energy growth of the perturbation $\boldsymbol{u}(x, y, t) = (u(x, y, t), v(x, y, t))$ is

$$E(t) = \int_0^L \int_0^H (|u|^2 + |v|^2)\,\mathrm{d}y\,\mathrm{d}x. \tag{3.3}$$

According to Schmid & Henningson (2001), the perturbation is sought as a linear superposition of the two-dimensional temporal modes

$$\boldsymbol{u}(x, y, t) = \sum_{k=1}^{N} \alpha_k(t)\hat{\boldsymbol{u}}_k(x, y). \tag{3.4}$$

The maximum of the energy at time t as function of all possible initial conditions is provided by

$$\max_{\alpha_k(0)} \frac{E(t)}{E(0)} = ||\boldsymbol{F}\exp(t\boldsymbol{D})\boldsymbol{F}^{-1}||^2 = G(t) \tag{3.5}$$

with $\boldsymbol{M} = \boldsymbol{F}^H\,\boldsymbol{F}$ the Cholesky decompostion of the Hermitian matrix $\boldsymbol{M}$ with entries

$$M_{ij} = \int_0^L \int_0^H (\hat{u}_i^*\hat{u}_j + \hat{v}_i^*\hat{v}_j)\,\mathrm{d}y\,\mathrm{d}x. \tag{3.6}$$

The diagonal matrix $\boldsymbol{D}$ contains the global eigenvalues and $\alpha_k(t) = \exp(-\mathrm{i}\omega_k t)\alpha_k(0)$ (see Schmid & Henningson 2001 for details). For both Reynolds numbers $Re = 610$ and 780, the spectrum for $L = 460$ has been considered, depicted as stars and triangles in figure 1, with respectively 20 and 22 eigenvalues. The complex conjugate eigenvalues $\sigma^* = \omega_i - \mathrm{i}\omega_r$, together with the complex conjugate eigenmodes, are to be considered as well, hence $N = 40$ and $N = 44$ has been taken in (3.4) for $Re = 610$ and $Re = 780$, respectively. The quantity $G(t)$ is depicted in figure 4 and while the result for $Re = 610$ only predicts a weak transient growth, at the higher Reynolds number $Re = 780$ the envelope reaches a peak at $t = 800$ with $G(t) \approx 7$.

In order to analyse the spatio-temporal development of optimal perturbations, the optimal initial condition for $Re = 780$ is determined at $t = 800$ and the perturbation

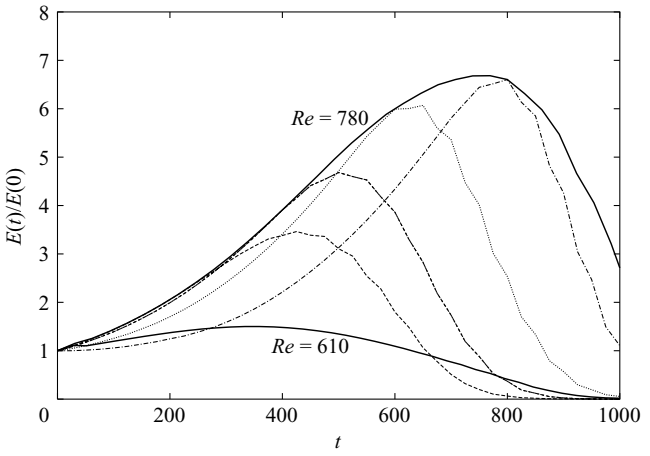

FIGURE 4. Optimal growth of the energy $G(t) = E(t)/E(0)$ as a function of time horizon t for $Re = 610$ and 780. The effective time-evolution of optimal perturbations for various time horizons is also plotted for $Re = 780$.

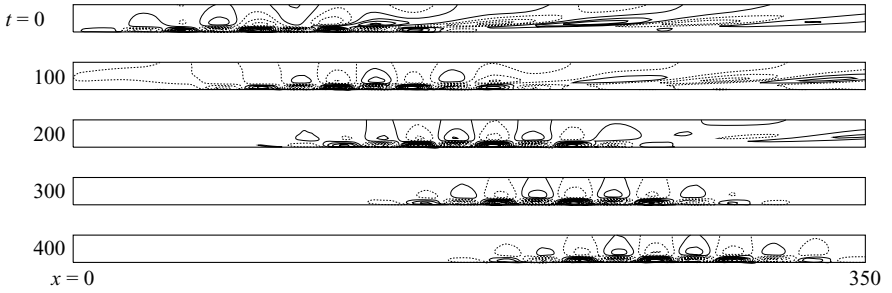

FIGURE 5. Spatio-temporal evolution of the wave packet associated with the optimal perturbation for $t = 800$ ($Re = 780$). Isolines of the real part of $\hat{u}(x, y)$ in the region $0 < x < 350$ and $0 < y < 12$ at various times. At each time, 20 equidistant levels have been considered, ranging from the minimum to the maximum value.

$\boldsymbol{u}(x, y, t)$ is easily computed through (3.4). The corresponding wave packet is shown in figure 5. The linear combination of the mode structures is shown to trigger a wave packet localized in space and moving along the plate for increasing time. Figure 5 demonstrates that the amplifying behaviour of the convectively unstable two-dimensional flat-plate boundary layer can be captured by a suitable superposition of two-dimensional temporal global modes, as suggested by the model analysis of Cossu & Chomaz (1997). Although the amplitude of the two-dimensional temporal modes is maximal near the outlet (see figure 2 and figure 3), their resulting non-orthogonal superposition produces a wave packet initially localized close to the inlet which grows in time and moves in space according to the phases of the individual modes, but ultimately decays as time increases and the wave packet leaves the domain. In figure 6(a), which depicts the spatio-temporal evolution of the perturbation amplitude with $||\boldsymbol{u}||(x, t) = (\int_0^H (u^2 + v^2)\,\mathrm{d}y)^{1/2}$, the dashed-dotted curve at time $t = 800$ further shows that the outflow boundary treatment described in § 2.1 is appropriate, letting the wave packet smoothly leave the plate.

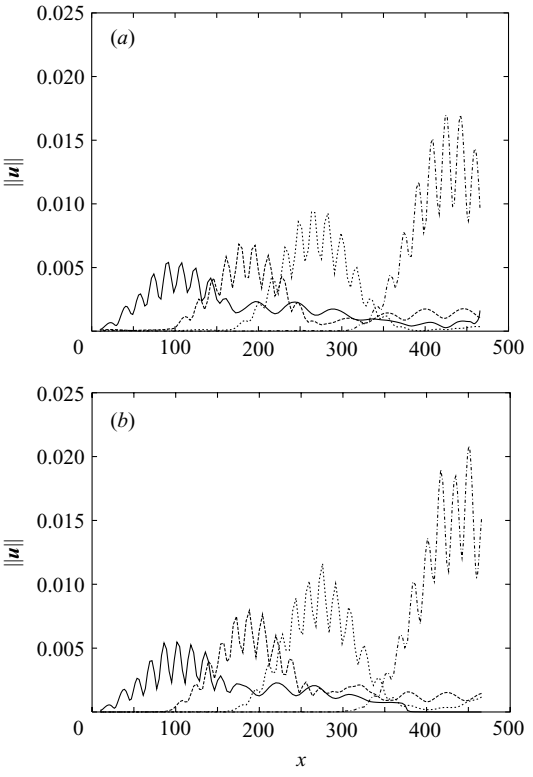

FIGURE 6. Spatio-temporal evolution of the wave packet amplitude triggered by the linear optimal perturbation for $t = 800$ at $t = 0$ (solid line), $t = 200$ (dashed line), $t = 400$ (dotted line) and $t = 800$ (dashed-dotted line). The time evolution is provided by the linear superposition of the global modes in (*a*) and by the DNS in (*b*).

To interpret the wave train as a genuine perturbation for the flat-plate boundary-layer flow, the initial condition $t = 0$ as provided by the analysis and depicted at the top of figure 5 has been superimposed on the basic state at $Re = 780$ and injected as initial condition with small amplitude into the Navier–Stokes solver. To compare the evolution at successive times, the amplitude $||\boldsymbol{u}||(x, t)$ has been computed along the plate and the comparison between the wave train as given by the perturbation expansion (3.4) and the disturbance provided by time integration of the Navier–Stokes system is depicted in figure 6. In the latter case the perturbation has been computed, subtracting from the instantaneous flow field the steady state at $Re = 780$. The wave train evolution compares quite well, the initial amplitude being chosen such that nonlinear effects when solving the full Navier–Stokes system are small. This comparison demonstrates that a perturbation expansion using the two-dimensional temporal mode analysis is reminiscent of the convective-type instability evolution.

4. Final remarks

It has been demonstrated that a finite number of two-dimensional temporal modes is capable of capturing the convective instability behaviour of the flat-plate boundary-layer. The associated weak transient temporal growth is of a different nature to the strong lift-up effect characteristic of wall-normal non-normality. Here, it is instead

triggered by the streamwise non-normality and the analysis provides a real flow example of what has been demonstrated so far for inhomogeneous one-dimensional model equations (Cossu & Chomaz 1997; Schmid & Henningson 2002). There is hence some evidence that a moderate number of two dimensional modes may reproduce the perturbation dynamics in wall-bounded open flows: this provides new possibilities for model reduction with flow-control applications.

We would like to acknowledge Carlo Cossu for enlightening discussions. We thank the anonymous referees for their advice concerning the wave packet simulation. The computations have been performed on the IDRIS NEC/SX5 under Grant 4055.

REFERENCES

Barkley, D., Gomes, M. & Henderson, D. H. 2002 Three-dimensional instability in flow over a backward-facing step. *J. Fluid Mech.* **473**, 167–189.

Chomaz, J.-M. 2005 Global instabilities in spatially developing flows: non-normality and nonlinearity. *Annu. Rev. Fluid Mech.* **37**, 357–392.

Cossu, C. & Chomaz, J.-M. 1997 Global measures of local convective instabilities. *Phys. Rev. Lett.* **78**, 4387–4390.

Edwards, W. S., Tuckerman, L. S., Friesner, R. A. & Sorensen, D. 1994 Krylov methods for the incompressible Navier-Stokes equations. *J. Comput. Phys.* **110**, 82–102.

Gaster, M. 1962 A note on the relation between temporally increasing and spatially increasing disturbances in hydrodynamic stability. *J. Fluid Mech.* **14**, 222–224.

Huerre, P. & Monkewitz, P. 1990 Local and global instabilities in spatially developing flows. *Annu. Rev. Fluid Mech.* **22**, 473–537.

Lin, R. S. & Malik, M. R. 1997 On the stability of attachment-line boundary layers. Part 2. The effect of leading edge curvature. *J. Fluid Mech.* **333**, 125–137.

Marquillie, M. & Ehrenstein, U. 2003 On the onset of nonlinear oscillations in a separating boundary-layer flow. *J. Fluid Mech.* **490**, 169–188.

Nayar, M. & Ortega, U. 1993 Computation of selected eigenvalues of generalized eigenvalues problems. *J. Comput. Phys.* **108**, 8–14.

Peyret, R. 2002 *Spectral Methods for Incompressible Viscous Flow*. Springer.

Schmid, P. J. & Henningson, D. S. 2001 *Stability and Transition in Shear Flows*. Springer.

Schmid, P. J. & Henningson, D. S. 2002 On the stability of a falling liquid curtain. *J. Fluid Mech.* **463**, 163–171.

Theofilis, V. 2003 Advances in global linear instability of nonparallel and three-dimensional flows. *Prog. Aerospace Sci.* **39**, 249–315.

Theofilis V., Hein, S. & Dallmann, U. 2000 On the origins of unsteadiness and three-dimensionality in a laminar separation bubble. *Phil. Trans. R. Soc. Lond.* A **358**, 3229–3246.